COMMUNICATION

Check for updates

On the Structural Stability of MXene and the Role of Transition Metal Adatoms†

Justinas Palisaitis, [ID] * Ingemar Persson, [ID] Joseph Halim, [ID] Johanna Rosen [ID] and Per O. Å. Persson [ID]

In the present communication, the atomic structure and coordination of surface adsorbed species on Nb_2C MXene is investigated over time. In particular, the influence of the Nb adatoms on the structural stability and oxidation behavior of the MXene is addressed. This investigation is based on the plane-view geometry observations of single Nb_2C MXene sheets by a combination of atomic-resolution scanning transmission electron microscopy (STEM), electron energy loss spectroscopy (EELS) and STEM image simulations.

Introduction

Two-dimensional (2D) transition metal carbides and/or nitrides (MXenes) constitute a rapidly growing new class of materials that present a wealth of chemistries and properties.[1,2] The parent material for obtaining MXene is the nanolaminated hexagonal MAX phase that follows the general formula $M_{n+1}AX_n$ (n = 1, 2 or 3), where M is a transition metal, A is a group 13 or 14 element, and X is C and/or N.[3–5] MAX phases are organized such that atomically thin A-element layers separate the sheets of $M_{n+1}X_n$.[6] To date, the parent MAX phase family constitutes well over 80 members,[4] not including solid solutions[7,8] or ordered double-M structures,[9–11] from which well over 20 different MXenes have been reported,[12] and the family is continuously growing.

MXenes are produced by targeted removal of the A element layer, typically Al, through chemical etching, realizing $M_{n+1}X_n$ sheets. After etching, the MXene can be described by the general formula $M_{n+1}X_nT_x$ where T_x stands for surface terminating functional groups that originate from the etchant. These termination groups, T_x, are predominantly oxygen (O) and fluorine (F) with smaller contributions from hydroxide (OH).[13,14] The large surface to volume ratio of the MXenes,

together with their extensive range of structures and chemistries, makes MXenes suitable for applications such as supercapacitors, batteries, transparent conducting electrodes, photocatalysts, water purification, electromagnetic shielding, and sensors among others.[12,15–24] Among MXenes, Nb_2C is a highly promising candidate as an electrode material in Li-ion batteries, maintaining the high capacity and handling high charge–discharge rates.[25–27] Furthermore, Nb_2CT_x have shown promising performance for photothermal cell ablation and as a photocatalyst for hydrogen evolution.[28–30]

Regardless of which MXene is investigated, these are typically oxidized with time under ambient conditions.[31–33] Thus, a fundamental understanding of the material stability, in particular with time and under ambient conditions, is crucial. Despite the progress in synthesis, property characterization and theoretical predictions, studies on the atomic level structural characterization of MXenes are scarce. STEM has previously been successfully implemented for atomic level investigation of MXenes.[34–36] The present study reports on the presence and coordination of Nb_2C surface adsorbed species, and their influence on the structural stability over time. The results were acquired using atomically resolved STEM imaging combined with EELS and STEM image simulations.

Experimental details

Nb_2CT_x MXene sheets were synthesized by selective etching of Al from Nb_2AlC.[27] The Nb_2AlC MAX phase powders were prepared by pressureless sintering and were afterwards immersed in 48% aqueous hydrofluoric acid to produce Nb_2CT_x multilayer MXene. To obtain Nb_2CT_x monolayers, the multilayer MXene powder was intercalated with tetrabutylammonium hydroxide (TBAOH) in water using the previously reported procedure[37] followed by delamination in water and sonication for 1 h, yielding less than 0.5 mg ml^{-1} suspension of colloidal MXene flakes in water. The complete synthesis details can be found in the ESI S1.†

Samples for STEM analysis were prepared by drop casting the obtained supernatant onto a lacey carbon film suspended

Thin Film Physics Division, Department of Physics, Chemistry and Biology (IFM), Linköping University, SE-581 83 Linköping, Sweden.
E-mail: justinas.palisaitis@liu.se

by copper TEM grids and drying it. The TEM sample was inserted immediately after drying into the microscope vacuum, hereafter referred to as 'fresh' throughout the manuscript. The same TEM sample was investigated again 5 days after synthesis, and after being stored in vacuum, as well as 6 days after synthesis. The sample was exposed to ambient conditions during the final day. Prior to each investigation, the sample was heated *in situ*, inside the TEM, for eliminating carbon contamination. TEM characterization was performed using the Linköping double Cs corrected FEI Titan[3] 60–300 operated at 300 kV. The elemental constituents of the MXene sheets were analysed by core-loss EELS. STEM image simulations were performed using the Dr Probe software[38] and employing microscope experimental parameters. Conditions for the STEM, EELS and STEM image simulations can be found in the ESI S2.†

Results and discussion

A typical low-magnification STEM image acquired from a single layer fresh Nb_2CT_x sheet along the [0001] *c*-axis is shown in Fig. 1a. The sheet exhibits large lateral dimensions

(>2 μm) and the homogeneous contrast suggests that the sheet is predominantly clean and uniformly thick. Previously, it was reported that TBAOH treatment can result in generating pores in MXene[39] (*e.g.*, Mo_2C), however, in this case no such structural features were observed, which is in line with a report on Ti_3CN MXenes obtained by the same synthesis method.[37] Fig. 1b shows the atomically-resolved STEM image of the Nb_2CT_x sheet, together with the corresponding Fast Fourier Transform (FFT). It appears that the Nb_2CT_x exhibits a highly ordered, close packed atomic structure, with additional complexes of apparent holes (dark) and high contrast atomic columns (bright) in an ordered mosaic. The observed atomic structure is unprecedented and does not resemble the honeycomb-like atomic arrangement expected from the Nb_2C MXene structure projected along the *c*-axis, see ESI S3.†

The STEM image acquired from the same TEM sample after being stored for 5 days in vacuum is shown in Fig. 1c. Surprisingly, the STEM image of the Nb_2CT_x structure now exhibits the expected honeycomb-like atomic arrangement as emphasized by FFT. Locally, the structure has also assumed a disordered appearance. An additional day (6 days after synthesis) of exposure to ambient conditions increased the disorder further, such that the honeycomb-like structure is
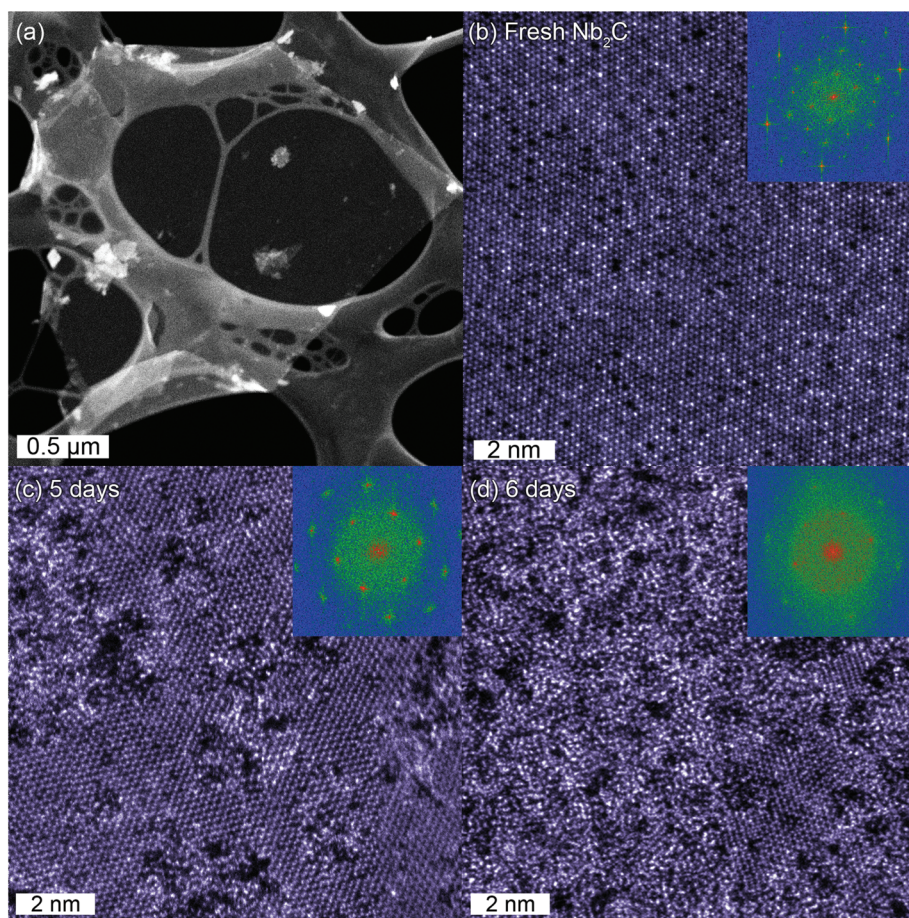

Fig. 1 (a) Overview of a single layer fresh Nb_2CT_x sheet. Atomically-resolved STEM images and the corresponding FFT patterns (insets) along the *c*-axis from (b) fresh, (c) 5 and (d) 6 days after synthesis.

retained only in small regions as shown in Fig. 1d. It should be stressed that at this point the 2D nature of the macroscopic sheet remains intact and that no indication of degradation is observed at lower magnifications (see ESI S4 and S5†).

In parallel to structural imaging, the elemental constituents and their evolution were monitored by EELS. The representative integrated and background-subtracted core-loss EELS spectra obtained from Nb_2CT_x are shown in Fig. 2. The obtained spectra were normalized with respect to the $Nb-M_{45}$ edge and vertically shifted with respect to each other for presentation purposes. It is found that the fresh Nb_2CT_x sheet was composed of Nb and C with O present, which is clearly indicated by $Nb-M_{45}$, C–K, and O–K absorption edges. Table 1 summarizes the relative amounts of Nb and O in the sample.

The C-edge intensity was fairly constant, yet it was excluded from the quantification due to potential C contamination which cannot be ignored. The presence of oxygen indicates that the surface is terminated by O and/or OH functional groups. No F was detected, see ESI S6.† The EELS spectra from the 5 and 6 day samples revealed a significant increase in the O content. In comparison, the Nb : O ratio increased from 2 : 1.4 to 2 : 7.4 and 2 : 9.7 for the fresh, 5 days and 6 days samples respectively. Consequently, the fresh sample includes less O than Nb while the latter samples display ∼4 times more O than Nb. The EELS data consequently indicate that the transformation from the ordered to disordered structure as seen in Fig. 1 is brought about by oxidation. In addition, the fresh sample has a Nb : O ratio which is substoichiometric for O.
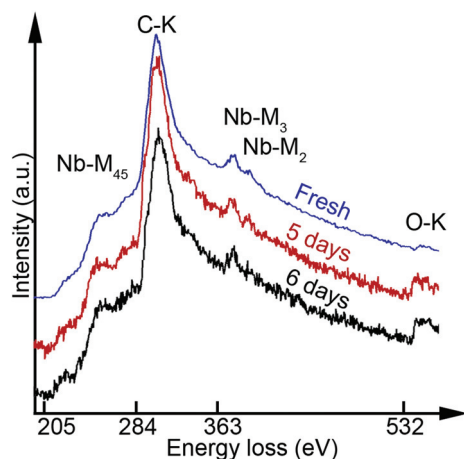

Fig. 2 Core-loss EELS spectra showing $Nb-M_{45}$, C–K, $Nb-M_3$, $Nb-M_2$ and O–K edges from the fresh Nb_2CT_x sheet as well as 5 and 6 days after the synthesis.

Table 1 Relative quantification of Nb and O in the sample

	Fresh	5 days	6 days
Nb (at%)	58.3	21.2	17.2
O (at%)	41.7	78.8	82.8
Nb : O	2 : 1.4	2 : 7.4	2 : 9.7

This is notable given that the M_2X MXene can accept one surface functional group per M atom, and that no F was observed in the sample. Still, this is in line with previous observations for $Ti_3C_2T_x$ which have clearly indicated that x can be well below 2.[34]

The fresh sample appearance looks like no previously observed M_2XT_x structure, and it is astonishing that it evolves into the regular M_2X appearance with time. To understand this behavior, it is essential to interpret the atomic structure of the fresh sample. Hence the STEM image (Fig. 3a) is divided into fundamental building blocks. Fig. 3b shows the M_2X *model structure* as projected along the *c*-axis and overlaid on the STEM image (Fig. 3a) by positioning the model honeycomb cores above the "holes" in the image. The model matches the image perfectly such that all "holes" are aligned on the honeycomb cores. Furthermore, the high intensity atomic columns also decorate the cores and do not coincide with the M atomic columns of the model structure. Additionally, some of the cores are hosting atoms of a similar intensity to those Nb atoms aligned with the model structure. The different columns are colour coded in Fig. 3c such that green, blue and pink represent model structure columns, high intensity columns and columns with an intensity equivalent to the model structure columns, respectively. It can also be observed that the high intensity atomic columns locally form a large honeycomb close packed pattern (indicated by red lines in Fig. 3c). Hence, the observed fresh sample's structure is based on the M_2X model structure with additional atomic columns of a similar or high intensity decorating the honeycomb cores.

To identify the nature of these additional atomic columns, STEM image simulations were performed. Core-loss EELS indicated the presence of Nb, C and O, but no F. Fully O terminated Nb_2C surfaces are considered throughout these simulations. This is motivated by a presumably immediate termination of the MXene surface from the etchant as the A layer is removed. It was previously reported that Nb_2C surfaces are hydrophilic and terminated mainly with OH groups after being etched in HF.[40] Theoretical calculations predict that the energetically favourable atomic sites for functional groups are located above the hollow site and pointed to Nb atoms (A-site) in the Nb_2C MXene.[40–42] This has also been theoretically predicted[41,42] and experimentally shown for Ti_3C_2 MXene,[34] hence this O termination site was presumed for the present simulations.

The structures used for the simulations are shown as side- and plane-views in Fig. 4, with the O terminated Nb_2C (Fig. 4a and d), an additional layer of Nb adatoms terminated with O on the top surface (Fig. 4b and e) and additional layers of Nb adatoms terminated with O on both surfaces (Fig. 4c and f). Simulations of additional Nb layers find relevance in the relatively high Nb content in the fresh Nb_2CT_x MXene sample. The additional Nb layers were positioned on hcp sites following the atomic arrangements in Nb_3C_2 and Nb_4C_3 layers of the corresponding Nb_3AlC_2 and Nb_4AlC_3 MAX phases. Note that in the two Nb layer simulation, both additional Nb adatoms are positioned in the same column, *i.e.* on top of each other (Fig. 4c
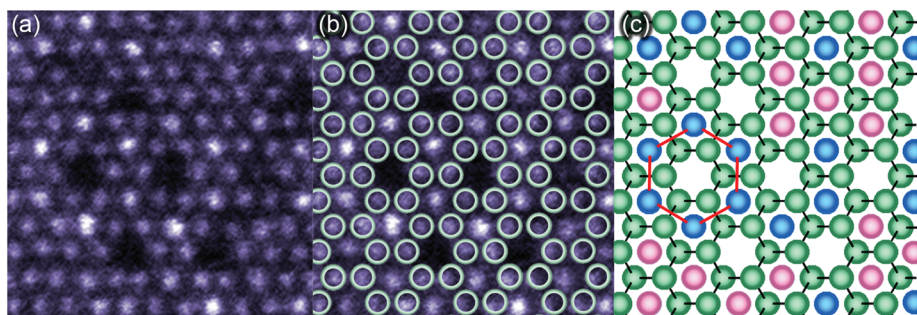
Fig. 3 (a) Atomically-resolved STEM image from the fresh Nb_2CT_x MXene, which is (b) with the M_2X model structure overlaid and (c) crystal structure sketch where the honeycomb cores filled with low (colored in pink) and high intensity atomic columns (blue). x (e.g., C) and T_x (e.g., O) are not shown in the model structure (b) and the sketch (c). High intensity atomic columns forming large honeycombs are indicated by red lines in (c).
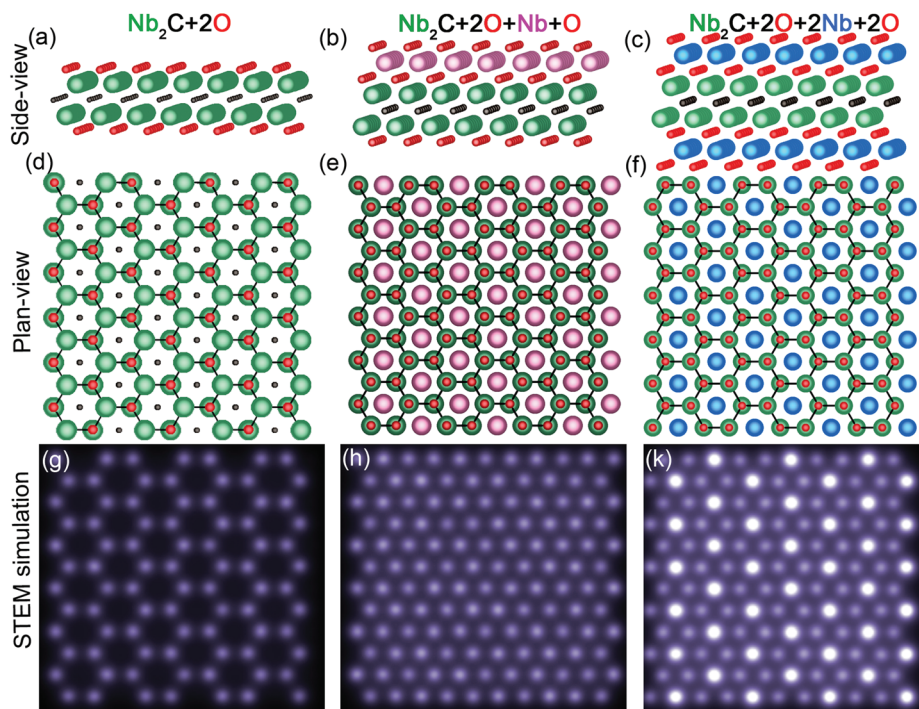

Fig. 4 Side-, plane-view crystal structure projections as well as STEM simulations for the model Nb_2C structure terminated by O (a, d, g), additionally decorated with a single Nb and O (b, e, h) as well as double Nb and O (c, f, k) layers.

and f). It should be noted that O adatoms on a Ti_3C_2 surface were found to be clearly visible.[34] In the present work, however, the simulated STEM images (Fig. 4g–k) exhibit distinct Nb (atomic number $Z = 41$) atom contrast, while the O ($Z = 8$) surface terminations are nearly invisible due to STEM image contrast dependence on $\sim Z^2$.[43]

As can be seen, the O terminated model structure returns to the expected honeycomb appearance in Fig. 4g (see also ESI S7†). Interestingly, the additional Nb layer results in a close-packed structure with atomic columns of similar intensity (Fig. 4h). Finally, the double Nb layer results in an image with high intensity atomic columns centred on the honeycomb cores (Fig. 4k). This close agreement between the experimental

and simulated STEM images suggests that the fresh Nb_2CT_x surfaces are decorated with Nb adatoms such that they are partially covering one or both surface sides of the Nb_2CT_x MXene.

Judging from Fig. 1b, the number of Nb adatoms on the MXene surface is remarkably high. By a rough approximation, based on Fig. 1b alone, 75% of each surface is covered by Nb adatoms and it is proposed that these are Nb adatoms that were adsorbed on the Nb_2CT_x surfaces during the applied etching, by complete or partial disintegration of adjacent MXene sheets. In strong contrast to other observations of MXenes,[34–36] the present example includes extensive amounts of adatoms. A high adsorption capacity of heavy metal adatoms on MXene surfaces was predicted by theoretical

means (*e.g.* Pb on V_2C) and corroborated through this investigation, although the absorption capacity was found to be influenced by the surface termination (T_x).[44]

Furthermore, it is suggested that this high amount of Nb adatoms is the direct cause of the gradual degradation observed throughout in Fig. 1. It was previously observed that Ti adatoms on Ti_3C_2 MXene attract O that together form highly mobile complexes.[34] It is inferred that the Nb adatoms increasingly attract additional O from the atmosphere (as corroborated by the EELS data), and then Nb and O complexes migrate on the MXene surface and agglomerate with time. While these clusters are formed, the Nb_2CT_x assume it's M_2X model structure appearance, as is seen in Fig. 1c. The oxidized Nb clusters are proposed to form unstable structures that locally destabilize the honeycomb Nb_2CT_x. Consequently, the Nb_2CT_x structure starts to disintegrate locally, which with time extends to include the entire sheet as observed in Fig. 1d. The implication for this required optimization of existing etching protocols is to prevent the adsorption of adatoms on the MXene surfaces, thereby increasing the stability of the MXene structures and extending the lifetime of potential MXene devices.

Conclusion

Single Nb_2CT_x MXene sheets were investigated in plane-view geometry by atomically resolved STEM, EELS and STEM simulations. It was found that for the applied etching protocol the resulting MXene surfaces were strongly decorated by Nb adatoms, positioned at hcp sites. It was shown that these adatoms attract and bond with ambient O, forming clusters that ripen over time. These clusters destabilize the MXene structure locally and eventually degrade the structure across the entire MXene sheet, while the sheet still retains its 2D nature. Consequently, the presence of adatoms on the MXene surfaces is detrimental for the long term structural stability, and should preferentially be reduced by optimized etching procedures.

Conflicts of interest

There are no conflicts to declare.

Acknowledgements

References

1 M. Naguib, M. Kurtoglu, V. Presser, J. Lu, J. J. Niu, M. Heon, L. Hultman, Y. Gogotsi and M. W. Barsoum, *Adv. Mater.*, 2011, **23**, 4248–4253.

2 M. Naguib, O. Mashtalir, J. Carle, V. Presser, J. Lu, L. Hultman, Y. Gogotsi and M. W. Barsoum, *ACS Nano*, 2012, **6**, 1322–1331.

3 M. W. Barsoum, *Prog. Solid State Chem.*, 2000, **28**, 201–281.

4 M. W. Barsoum, *MAX Phases: Properties of Machinable Ternary Carbides and Nitrides*, John Wiley & Sons, 2013.

5 P. Eklund, J. Rosén and P. O.Å. Persson, *J. Phys. D: Appl. Phys.*, 2017, **50**, 113001.

6 M. Naguib and Y. Gogotsi, *Acc. Chem. Res.*, 2015, **48**, 128–135.

7 M. Naguib, G. W. Bentzel, J. Shah, J. Halim, E. N. Caspi, J. Lu, L. Hultman and M. W. Barsoum, *Mater. Res. Lett.*, 2014, **2**, 233–240.

8 B. Manoun, S. Saxena, G. Hug, A. Ganguly, E. Hoffman and M. W. Barsoum, *J. Appl. Phys.*, 2007, **101**, 113523.

9 Q. Tao, M. Dahlqvist, J. Lu, S. Kota, R. Meshkian, J. Halim, J. Palisaitis, L. Hultman, M. W. Barsoum, P. O. Å. Persson and J. Rosen, *Nat. Commun.*, 2017, **8**, 14949.

10 M. Dahlqvist, J. Lu, R. Meshkian, Q. Tao, L. Hultman and J. Rosen, *Sci. Adv.*, 2017, **3**, 1700642.

11 J. Lu, A. Thore, R. Meshkian, Q. Tao, L. Hultman and J. Rosen, *Cryst. Growth Des.*, 2017, **17**, 5704–5711.

12 V. M. H. Ng, H. Huang, K. Zhou, P. S. Lee, W. Que, J. Z. Xu and L. B. Kong, *J. Mater. Chem. A*, 2017, **5**, 3039.

13 H. W. Wang, M. Naguib, K. Page, D. J. Wesolowski and Y. Gogotsi, *Chem. Mater.*, 2016, **28**, 349–359.

14 J. Halim, K. M. Cook, M. Naguib, P. Eklund, Y. Gogotsi, J. Rosen and M. W. Barsoum, *Appl. Surf. Sci.*, 2016, **362**, 406–417.

15 M. R. Lukatskaya, S. Kota, S. Z. Lin, M.-Q. Zhao, N. Shpigel, M. D. Levi, J. Halim, P.-L. Taberna, M. W. Barsoum and P. Simon, *Nat. Energy*, 2017, **2**, 17105.

16 J. Halim, M. R. Lukatskaya, K. M. Cook, J. Lu, C. R. Smith, L.-Å. Näslund, S. J. May, L. Hultman, Y. Gogotsi and P. Eklund, *Chem. Mater.*, 2014, **26**, 2374–2381.

17 M. Naguib, V. N. Mochalin, M. W. Barsoum and Y. Gogotsi, *Adv. Mater.*, 2014, **26**, 992–1005.

18 B. Anasori, M. R. Lukatskaya and Y. Gogotsi, *Nat. Rev. Mater.*, 2017, **2**, 16098.

19 P. Eklund, J. Rosen and P. O. Å. Persson, *J. Phys. D: Appl. Phys.*, 2017, **50**, 113001.

20 N. K. Chaudhari, H. Jin, B. Kim, D. S. Baek, S. H. Joo and K. Lee, *J. Mater. Chem. A*, 2017, **5**, 24564–24579.

21 J. Zhu, E. Ha, G. Y. Zhao, Y. D. Huang, G. Yue, L. Hu, N. Sun, Y. Wang, L. Y. S. Lee, C. Xu, K.-Y. Wong, D. Astruc and P. Zhao, *Coord. Chem. Rev.*, 2017, **352**, 306–327.

22 J. Zhang, S. Seyedin, Z. Gu, W. Yang, X. Wanga and J. M. Razal, *Nanoscale*, 2017, **9**, 18604.

23 B. Ahmed, D. H. Anjum, M. N. Hedhili, Y. Gogotsi and H. N. Alshareef, *Nanoscale*, 2016, **8**, 7580–7587.

24 I. Persson, A. Ghazaly, Q. Tao, J. Halim, S. Kota, V. Darakchieva, J. Palisaitis, M. W. Barsoum, P. O. Å. Persson and J. Rosen, *Small*, 2018, 1703676–1703683.

25 J. Halim, J. Palisaitis, J. Lu, J. Thörnberg, E. J. Moon, M. Precner, P. Eklund, P. O. Å. Persson, M. W. Barsoum and J. Rosen, *ACS Appl. Nano Mater.*, 2018, DOI: 10.1021/acsanm.8b00332.

26 O. Mashtalir, M. R. Lukatskaya, M. Q. Zhao, M. W. Barsoum and Y. Gogotsi, *Adv. Mater.*, 2015, **27**, 3501–3506.

27 M. Naguib, J. Halim, J. Lu, K. M. Cook, L. Hultman, Y. Gogotsi and M. W. Barsoum, *J. Am. Chem. Soc.*, 2013, **135**, 15966–15969.

28 H. Lin, S. Gao, C. Dai, Y. Chen and J. Shi, *J. Am. Chem. Soc.*, 2017, **139**, 16235–16247.

29 T. Su, R. Peng, Z. D. Hood, M. Naguib, I. N. Ivanov, J. K. Keum, Z. Qin, Z. Guo and Z. Wu, *ChemSusChem*, 2018, **11**, 1–13.

30 A. Byeon, A. M. Glushenkov, B. Anasori, P. Urbankowski, J. Li, B. W. Byles, B. Blake, K. L. Van Aken, S. Kota, E. Pomerantseva, J. W. Lee, Y. Chen and Y. Gogotsi, *J. Power Sources*, 2016, **326**, 686–694.

31 O. Mashtalir, K. M. Cook, V. N. Mochalin, M. Crowe, M. W. Barsoum and Y. Gogotsi, *J. Mater. Chem. A*, 2014, **2**, 14334.

32 A. Lipatov, M. Alhabeb, M. R. Lukatskaya, A. Boson, Y. Gogotsi and A. Sinitskii, *Adv. Electron. Mater.*, 2016, **2**, 1600255.

33 C. J. Zhang, S. Pinilla, N. McEvoy, C. P. Cullen, B. Anasori, E. Long, S.-H. Park, A. Seral-Ascaso, A. Shmeliov, D. Krishnan, C. Morant, X. Liu, G. S. Duesberg, Y. Gogotsi and V. Nicolosi, *Chem. Mater.*, 2017, **29**, 4848–4856.

34 I. Persson, L.-Å. Näslund, J. Halim, M. W. Barsoum, V. Darakchieva, J. Palisaitis, J. Rosen and P. O.Å. Persson, *2D Mater.*, 2018, **5**, 015002.

35 L. Karlsson, J. Birch, J. Halim, M. W. Barsoum and P. O. Å. Persson, *Nano Lett.*, 2015, **15**, 4955–4960.

36 X. Sang, Y. Xie, M.-W. Lin, M. Alhabeb, K. L. Van Aken, Y. Gogotsi, P. R. C. Kent, K. Xiao and R. R. Unocic, *ACS Nano*, 2016, **10**, 9193–9200.

37 M. Naguib, R. R. Unocic, B. L. Armstronga and J. Nandaa, *Dalton Trans.*, 2015, **44**, 9353–9358.

38 J. Barthel, *Dr. Probe – High-resolution (S)TEM image simulation software*, 2017.

39 J. Halim, S. Kota, M. R. Lukatskaya, M. Naguib, M.-Q. Zhao, E. J. Moon, J. Pitock, J. Nanda, S. J. May, Y. Gogotsi and M. W. Barsoum, *Adv. Funct. Mater.*, 2016, **26**, 3118–3127.

40 Y. Xie, M. Naguib, V. N. Mochalin, M. W. Barsoum, Y. Gogotsi, X. Yu, K.-W. Nam, X.-Q. Yang, A. I. Kolesnikov and P. R. C. Kent, *J. Am. Chem. Soc.*, 2014, **136**, 6385–6394.

41 A. N. Enyashin and A. L. Ivanovskii, *Comput. Theor. Chem.*, 2012, **989**, 27–32.

42 Q. Tang, Z. Zhou and P. Shen, *J. Am. Chem. Soc.*, 2012, **34**, 16909–16916.

43 O. L. Krivanek, M. F. Chisholm, V. Nicolosi, T. J. Pennycook, G. J. Corbin, N. Dellby, M. F. Murfitt, C. S. Own, Z. S. Szilagyi, M. P. Oxley, S. T. Pantelides and S. J. Pennycook, *Nature*, 2010, **464**, 571–574.

44 X. Guo, X. Zhang, S. Zhao, Q. Huang and J. Xue, *Phys. Chem. Chem. Phys.*, 2016, **18**, 228.